ARTICLES
https://doi.org/10.1038/s41559-018-0728-7
nature ecology & evolution

Pterosaur integumentary structures with complex feather-like branching

Zixiao Yang[1], Baoyu Jiang[1*], Maria E. McNamara[2], Stuart L. Kearns[3], Michael Pittman[4], Thomas G. Kaye[5], Patrick J. Orr[6], Xing Xu[7] and Michael J. Benton[3*]

Pterosaurs were the first vertebrates to achieve true flapping flight, but in the absence of living representatives, many questions concerning their biology and lifestyle remain unresolved. Pycnofibres—the integumentary coverings of pterosaurs—are particularly enigmatic: although many reconstructions depict fur-like coverings composed of pycnofibres, their affinities and function are not fully understood. Here, we report the preservation in two anurognathid pterosaur specimens of morphologically diverse pycnofibres that show diagnostic features of feathers, including non-vaned grouped filaments and bilaterally branched filaments, hitherto considered unique to maniraptoran dinosaurs, and preserved melanosomes with diverse geometries. These findings could imply that feathers had deep evolutionary origins in ancestral archosaurs, or that these structures arose independently in pterosaurs. The presence of feather-like structures suggests that anurognathids, and potentially other pterosaurs, possessed a dense filamentous covering that probably functioned in thermoregulation, tactile sensing, signalling and aerodynamics.

Feathers are the most complex integumentary appendages in vertebrates[1]. Most feathers in modern birds possess an axial shaft from which lateral barbs and barbules branch. Much is known about the anatomy, developmental biology and genomic regulation of these structures, but their deep evolutionary origin is controversial[2–4]. Feathers and feather-like integumentary structures have been reported in many theropod dinosaurs (including birds)[3,5] and ornithischians, such as *Psittacosaurus*[6], *Tianyulong*[7] and *Kulindadromeus*[8]. Feather- or hair-like structures, termed pycnofibres[9], have also been reported in several pterosaur specimens[9–13], but their nature is not resolved.

Here, we report remarkably well-preserved pycnofibres in two anurognathid pterosaurs, and demonstrate—using evidence from morphology, chemistry and macroevolutionary analyses—that the preserved pycnofibres bear key features of feathers: monofilaments, two types of non-vaned grouped filaments, bilaterally branched filaments that were previously considered unique to maniraptoran dinosaurs, and preserved melanosomes with diverse geometries. Both specimens studied are from the Middle–Late Jurassic Yanliao Biota (around 165–160 million years ago[14]). NJU–57003 (Nanjing University) is a newly excavated specimen from the Mutoudeng locality. CAGS–Z070 (Institute of Geology, Chinese Academy of Geological Sciences), which has been noted briefly for its feather-like branched pycnofibres[13], is from the Daohugou locality. Both specimens are near-complete and well-articulated, with extensive soft tissues (Figs. 1 and 2 and Supplementary Figs. 1–5). Both specimens are identified as anurognathids[15] (see Supplementary Text for osteological descriptions).

Preserved soft tissues include structural fibres (actinofibrils) and pycnofibres. Structural fibres—common in the pterosaur wing membrane[9,12,16]—are observed only in the posterior portion of the uropatagium in CAGS–Z070 (Fig. 1o,p). As reported elsewhere, they are parallel to subparallel and closely packed. Individual fibres are 0.08–0.11 mm wide (around 5 fibres per mm) and at least 1.9 mm long. Pycnofibres are preserved extensively in both pterosaur specimens (especially CAGS–Z070; Figs. 1 and 2 and Supplementary Figs. 1, 4 and 5) and are discriminated from structural fibres based on their curved morphology and overlapping arrangement. In the posterior portion of the uropatagium in CAGS–Z070, pycnofibres co-occur with structural fibres; oblique intersections reflect superposition of these features during decay (Fig. 1o,p).

Pycnofibres are categorized here into four types. Type 1 occurs around the head, neck, shoulder, torso, all four limbs and tail of both specimens (Figs. 1c–e,o,p and 2b,c,f). It comprises curved monofilaments that are 3.5–12.8 mm long and 70–430 µm wide. Some short, distally tapering examples discriminate between dark-toned lateral margins and light-toned axial regions, especially near the filament base where the light-toned axis is wider, suggesting a tube-like morphology (Fig. 1c–e). Type 2 is preserved in the neck, proximal forelimb, plantar metatarsus and proximal tail regions of CAGS–Z070. It consists of bundles of curved filaments of similar length that appear to form brush-like structures at the distal ends of thicker filaments (2.0–13.8 mm long and 80–180 µm wide) (Fig. 1f–h). These brush-like structures may represent individual thick filaments or fused proximal regions of thinner distal filaments. Type 3 occurs around the head of CAGS–Z070. It comprises straight to slightly curved, distally tapered, central filaments (4.5–7.0 mm long and 50–450 µm wide) with short lateral branches that diverge from the central filament near the midpoint (Fig. 1i–k). There are five type 3 filaments identified on the head, next to five similar filaments that are probably of the same nature but obscured by overlapping filaments (Supplementary Fig. 5b). Type 4 occurs on the wing membrane of

[1]Center for Research and Education on Biological Evolution and Environments, School of Earth Sciences and Engineering, Nanjing University, Nanjing, China. [2]School of Biological, Earth and Environmental Sciences, University College Cork, Cork, Ireland. [3]Department of Earth Sciences, University of Bristol, Bristol, UK. [4]Vertebrate Palaeontology Laboratory, Department of Earth Sciences, University of Hong Kong, Pokfulam, China. [5]Foundation for Scientific Advancement, Sierra Vista, AZ, USA. [6]UCD School of Earth Sciences, University College Dublin, Dublin, Ireland. [7]Key Laboratory of Vertebrate Evolution and Human Origins, Institute of Vertebrate Paleontology and Paleoanthropology, Chinese Academy of Sciences, Beijing, China.
*e-mail: byjiang@nju.edu.cn; mike.benton@bristol.ac.uk

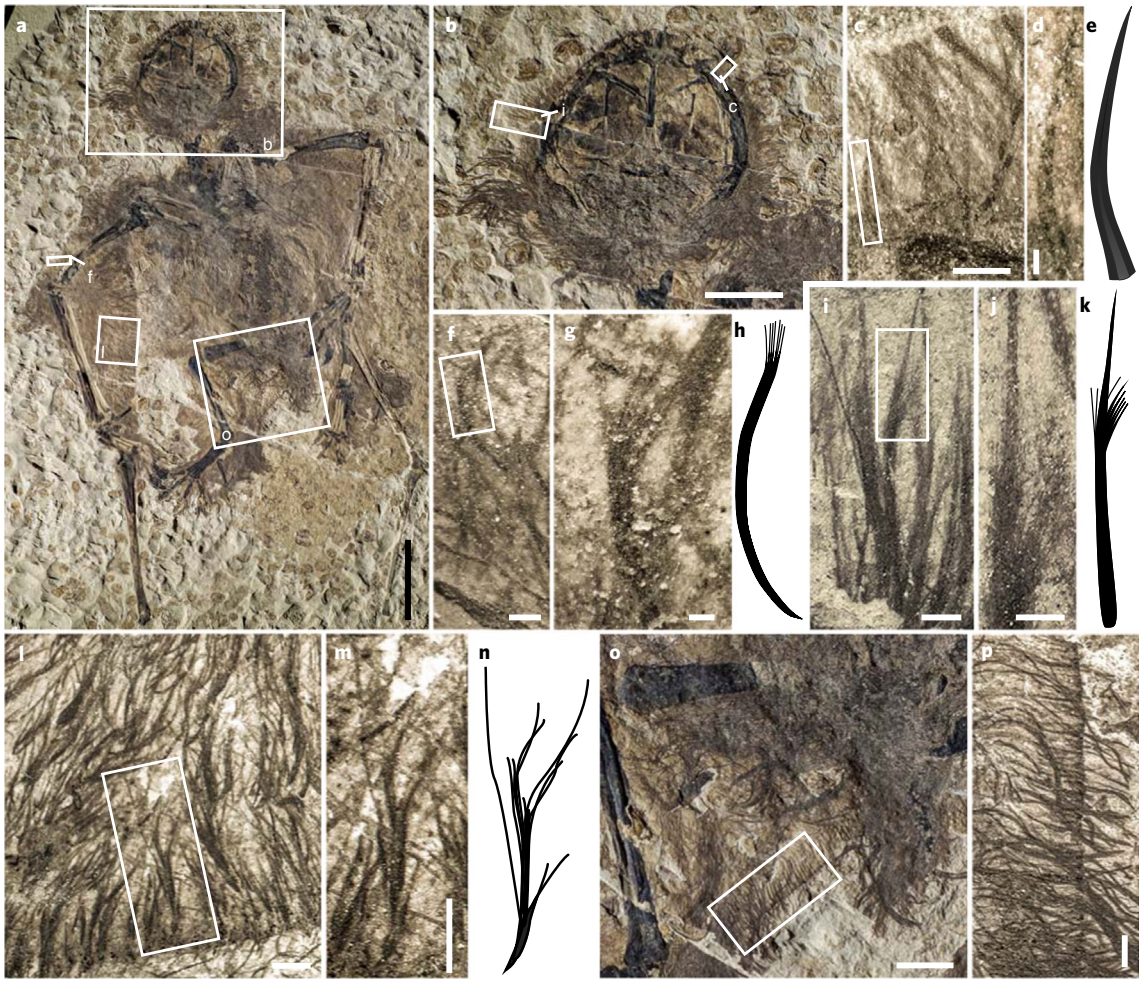

Fig. 1 | Integumentary filamentous structures in CAGS-Z070. a, Overview, showing extensive preservation of soft tissues. **b**–**p**, Details of the integumentary filaments in the regions indicated in **a** on the head and neck (**b**–**d**, **i** and **j**), forelimb (**f** and **g**), wing (**l** and **m**) and tail (**o** and **p**), and illustrated reconstructions of the filaments (type 1 filament (**e**), type 2 filament (**h**), type 3 filament (**k**) and type 4 filament (**n**)). Scale bars: 20 mm in **a**, 10 mm in **b**, 500 μm in **c** and **i**, 100 μm in **d**, 1 mm in **f**, **l**, **m** and **p**, 200 μm in **g** and **j**, and 5 mm in **o**.

both specimens. It comprises tufts of curved filaments (2.5–8.0 mm long and 70–130 μm wide) that diverge proximally (Figs. 1l–n and 2d,e), in contrast with the clear separation between type 1 filaments (Fig. 1o,p).

Filamentous integumentary structures in extant and fossil vertebrates commonly contain melanin-bearing organelles (melanosomes). Scanning electron microscopy (SEM) of the filamentous structures of NJU–57003 reveals densely packed microbodies 0.70 ± 0.11 μm long and 0.32 ± 0.05 μm wide (Fig. 2g,h, Supplementary Figs. 4a–f, 6 and 7 and Supplementary Table 2). As with most melanosome-rich fossil feathers[17–19], energy-dispersive X-ray spectroscopy spectra of the filaments are dominated by a major peak for carbon (Supplementary Fig. 8). These carbonaceous microbodies resemble fossil melanosomes in terms of their geometry, dense packing, parallel alignment relative to the long axis of the integumentary structure (that is, barbules in Paraves) and preservation within the matrix of the filament (see Supplementary Text). Most of the microbodies are oblate and morphologically similar to those that are usually interpreted as phaeomelanosomes in fossils[17] (Fig. 2h). Rod-shaped examples—usually interpreted as eumelanosomes in fossils[17] (Fig. 2g)—are rare.

Fourier transform infrared spectroscopy (FTIR) of samples of pterosaur filaments shows four major peaks unique to the filaments (Fig. 2i). These peaks are consistent with the absorption regions of amide I at around 1,650 cm^{-1} (principally the C=O asymmetric stretching vibration with some C–N bending), amide II at around 1,540 cm^{-1} (a combination of N–H in-plane bending and C–N and C–C stretching, as in indole and pyrrole in melanin and amino acids) and aliphatic C–H stretching at 2,850 and 2,918 cm^{-1} (ref. [20]). These peaks also occur in spectra obtained from extant feathers[19,21], fossil feathers of the paravian *Anchiornis*[18], and melanosomes isolated from human hair[22]. Furthermore, spectra of the pterosaur filaments more closely resemble those of pheomelanin-rich red human hair in the stronger absorption regions at around 2,850 and 2,918 cm^{-1} and higher-resolution spectra in the region around 1,500–1,700 cm^{-1} than those from eumelanin-rich black human hair and the ink sac of cuttlefish[22]. This, together with the SEM results, suggests that the densely packed microbodies in the pterosaur filaments are preserved melanosomes. The amide I peak at 1,650 cm^{-1} is more consistent with α-keratin (characteristic of extant mammal hair[23]) than β-keratin (the primary keratin in extant avian feathers[20,24]). This signal may be original or diagenetic; the molecular configuration of keratin[24] and other proteins[25] can alter under mechanical stress and changes in hydration levels.

The ultrastructural and chemical features of the pterosaur filaments confirm that they are hair- or feather-like integumentary structures. The four types of filaments described here show distinct distributions and morphologies. They are clearly separated from

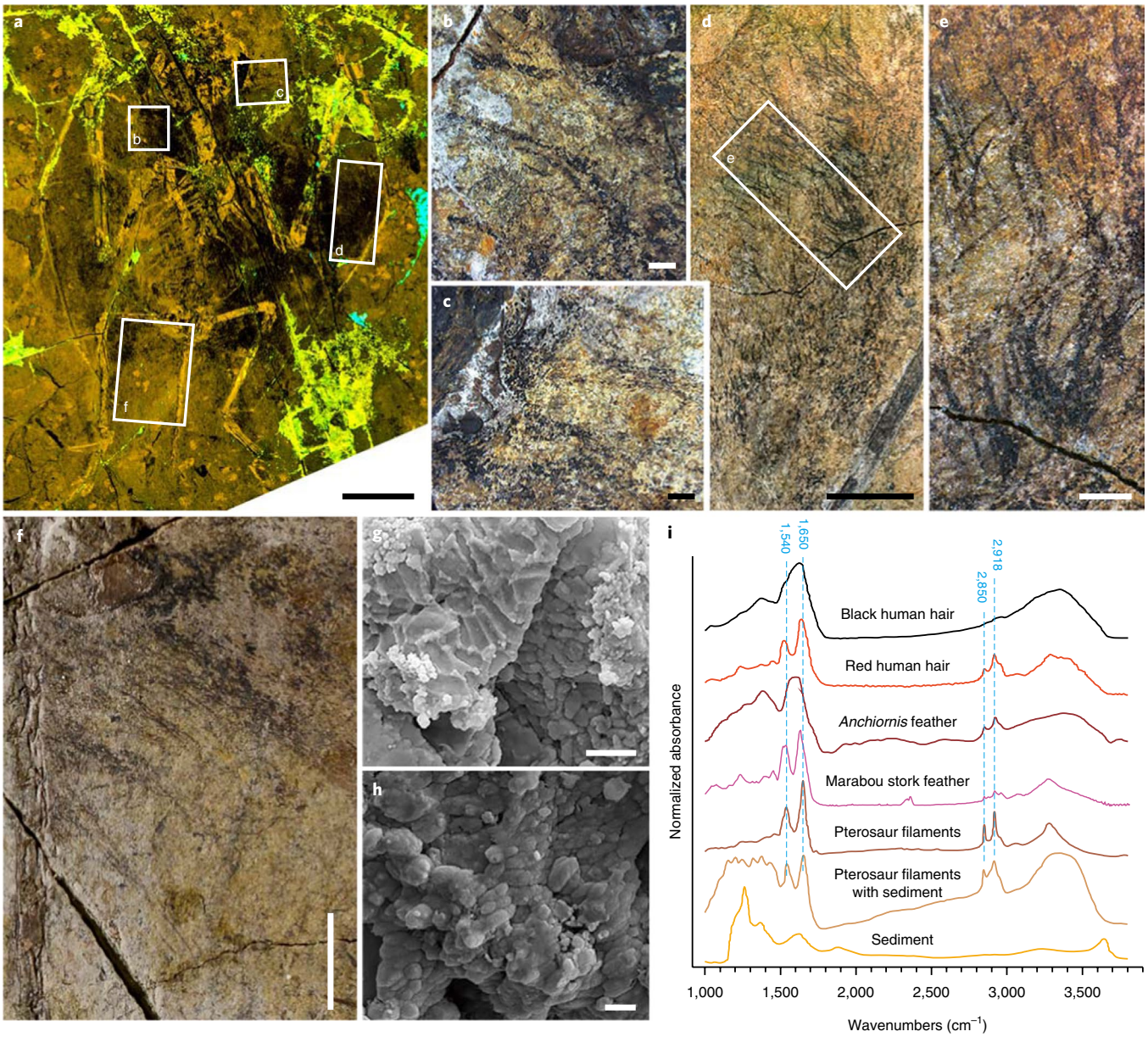

Fig. 2 | Preservation, microstructure and chemistry of the integumentary filamentous structures in NJU-57003. a, Laser-stimulated fluorescence[6,40,41] imaging highlights extensive preservation of the soft tissues (black areas). **b**–**f**, Details of the integumentary filaments in the regions indicated in **a** on the head and neck (**b** and **c**), wing (**d** and **e**) and tail (**f**). **g**,**h**, Scanning electron micrographs of the monofilaments on the neck (sample 10; **g**) and hindlimb (sample 39; **h**) (Supplementary Fig. 1a) show densely packed, elongate and oblate melanosomes. **i**, FTIR absorbance spectra of the monofilaments, monofilaments with sediment matrix, and sediment matrix in NJU-57003 (Sample 15; Supplementary Fig. 1a) compared with spectra from a feather of *Anchiornis* (from ref. [18]), an extant Marabou stork feather (from ref. [19]), and black and red human hair melanosomes (from ref. [22]). Scale bars: 20 mm in **a**, 1 mm in **b**, **c** and **e**, 5 mm in **d** and **f**, and 1 μm in **g** and **h**.

the sedimentary matrix by sharp boundaries (Supplementary Fig. 4g–i). There is no evidence that one or more filament type(s) were generated taphonomically (for example, through selective degradation or fossilization, or superimposition of filaments). For instance, although type 1 and 4 filaments occur widely in both specimens, type 4 occurs only in the wings, while type 1 occupies the remaining body regions. Type 1 filaments are thus not degraded products of type 4, and type 4 filaments do not represent superimposed clusters of type 1 filaments. Filament types 2 and 3 occur only in CAGS–Z070. Type 3 occurs only in the facial area and is associated with type 1, where types 2 and 4 are not evident. Type 3 filaments are thus not degraded type 2 or 4 filaments. Central filaments of type 3 are morphologically identical to the short, distally tapering filaments of type 1, but the branching filaments are much thinner (<40 μm for type 3 versus >70 μm for type 1) and shorter (<0.6 mm versus >3.5 mm, respectively) than the type 1 filaments. The branching filaments are thus unlikely to reflect superimposition of clusters of type 1 filaments. In contrast, the distal ends of type 2 filaments are similar, and have a similar distribution pattern, to type 1 filaments. An alternative interpretation—that type 2 filaments might represent superimposition of type 1 filaments at their proximal ends—is unlikely (see detailed discussion in the Supplementary Text). Feathers and feather-like integumentary structures have been reported in non-avian dinosaurs, although debate continues about

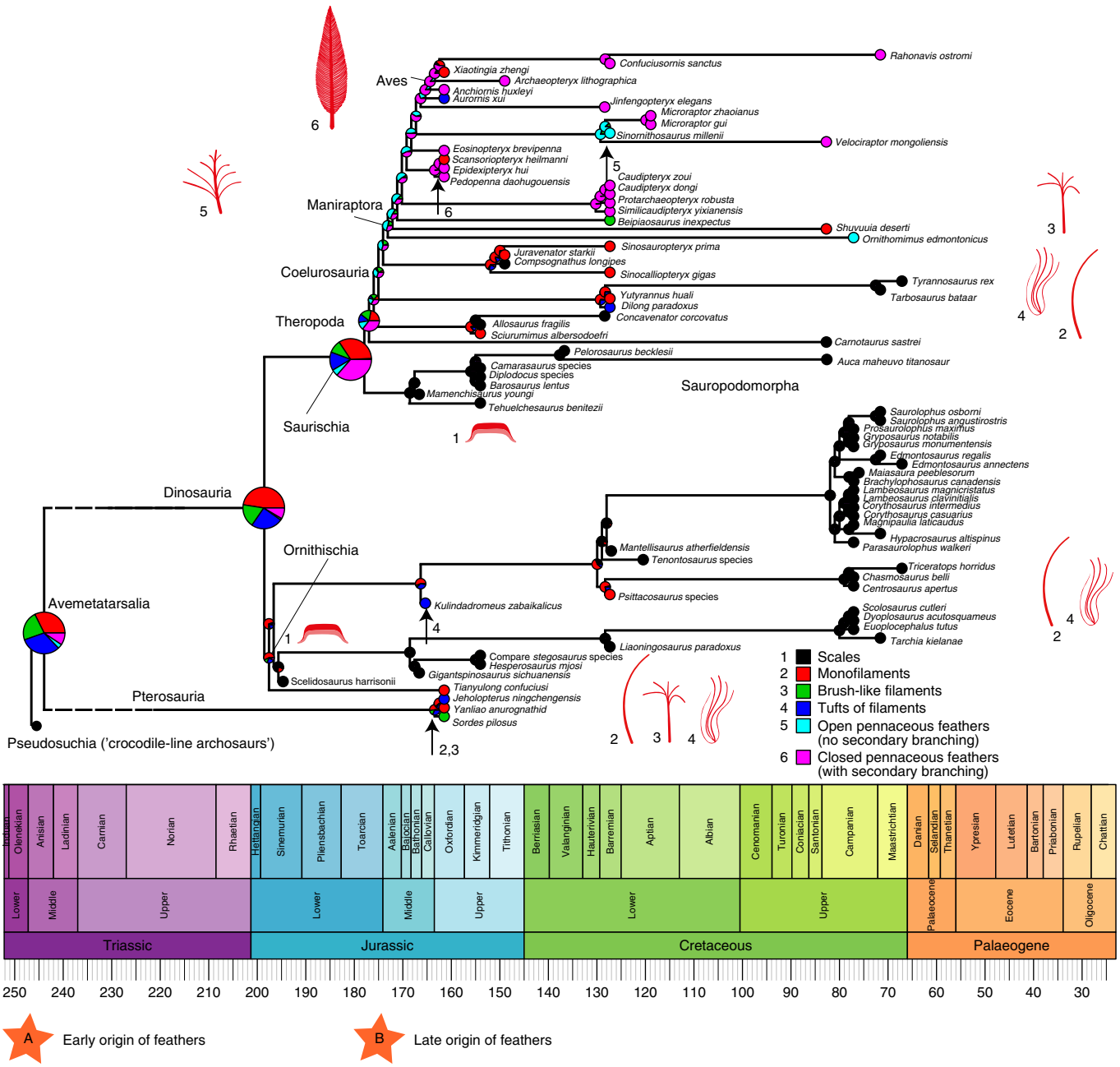

Fig. 3 | Phylogenetic comparative analysis of integumentary filament and feather evolution in pterosaurs and archosaurs. The phylogeny is scaled to geological time, with recorded terminal character states for each species and estimated ancestral character states at the lower nodes. This model is the most likely of the maximum-likelihood models, based on minimum branch lengths and transitions occurring as all-rates-different, but other results with lower likelihoods show scales as ancestral. The ancestral state reconstruction shows a combination of monofilaments, tuft-like filaments and brush-type filaments as the ancestral state for Avemetatarsalia and Dinosauria. The estimated ancestral state for Theropoda comprises all five feather states. Numbered small vertical arrows indicate the earliest occurrences of feather types 2–6. Two hypotheses for the timing of avian feather origins are indicated: early origin, at the base of Avemetatarsalia in the Early Triassic (A) or late origin, at the base of Maniraptora in the Early–Middle Jurassic (B).

their true nature[2]. These structures have been ascribed to several morphotypes—some absent in living birds[3,5]—and provide a basis to analyse the evolutionary significance of pterosaur pycnofibres. The pterosaur type 1 filaments resemble monofilaments in the ornithischian dinosaurs *Tianyulong* and *Psittacosaurus* and the coelurosaur *Beipiaosaurus*: unbranched, cylindrical structures with a midline groove that widens towards the base (presumed in *Beipiaosaurus*)[3,5]. The pterosaur type 2 filaments resemble the brush-like bundles of filaments in the coelurosaurs *Epidexipteryx* and *Yi*[3,5,26]: both comprise parallel filaments that unite proximally. The morphology and circumcranial distribution of pterosaur type 3 filaments resemble bristles in modern birds[1], but surprisingly do not correspond to any reported morphotype in non-avian dinosaurs. The type 3 filaments recall bilaterally branched filaments in *Sinornithosaurus*, *Anchiornis* and *Dilong*, but type 3 filaments in *Dilong* branch throughout their length, rather than halfway along the central filament(s), as in the pterosaur structure[3,5]. The pterosaur type 4 filaments are identical to the radially branched, downy feather-like morphotype found widely in coelurosaurs such as *Sinornithosaurus*, *Beipiaosaurus*, *Protarchaeopteryx*, *Caudipteryx* and *Dilong*[3,5].

Fig. 4 | Reconstruction of one of the studied anurognathid pterosaurs. This pterosaur exhibits diverse types of pycnofibres distributed in different body parts. Credit: Yuan Zhang

The filamentous integumentary structures in our anurognathid pterosaurs are thus remarkably similar to feathers and feather-like structures in non-avian dinosaurs. Intriguingly, cylindrical (type 1), radially symmetrical branched (types 2 and 4) and bilaterally symmetrical branched (type 3) filaments clearly coexisted in individual animals; these structures may represent transitional forms in the evolution of feathers, as revealed by developmental studies[3,5]. These new findings warrant revision of the origin of complex feather-like branching integumentary structures from Dinosauria to Avemetatarsalia (the wider clade that includes dinosaurs, pterosaurs and close relatives)[4,27]. The early evolutionary history of bird feathers and homologous structures in dinosaurs, and the multiple complex pycnofibres of pterosaurs, is enigmatic. A previous study concluded that the common ancestor of these clades bore scales and not filamentous integumentary appendages[2], but this result emerged only when the filaments of pterosaurs were coded as non-homologous with those of dinosaurs and there are no morphological criteria for such a determination. The presence of multiple pycnofibre types and their morphological, ultrastructural and chemical similarity to feathers and feather-like structures in various dinosaurian clades confirms their probable homology with filamentous structures in non-avian dinosaurs and birds. Comparative phylogenetic analysis produces equivocal results: maximum-likelihood modelling of plausible ancestral states against various combinations of branch length and character transition models (Supplementary Text, Supplementary Fig. 9 and Supplementary Table 3) reveals various potential solutions. The statistically most likely result (Fig. 3 and Supplementary Table 3; highest log-likelihood value) shows that the avemetatarsalian ancestors of dinosaurs and pterosaurs possessed integumentary filaments, with the highest likelihood of possessing monofilaments; tufts of filaments (especially brush-type filaments) are less likely ancestral states. This confirms that feather-like structures arose in the Early or Middle Triassic. The alternative tree for Dinosauria, with Ornithischia and Theropoda paired as Ornithoscelida[28], produces an identical result.

Present these modelling data with caution for two reasons: (1) the tree rooting method can influence the result (Supplementary Table 3), favouring results in which either scales are the basal condition or non-theropod feather-like structures and feathers evolved independently (Supplementary Fig. 9 and Supplementary Table 3); and (2) there is no adequate way to model the probabilities of evolution of all six feather types, or to model the probabilities of transitions between the six different feather types.

The discovery of multiple types of feather-like structures in pterosaurs has broad implications for our understanding of pterosaur biology and the functional origin of feather-like structures in Avemetatarsalia[29,30]. Potential functions of these structures include insulation, tactile sensing, streamlining and colouration (primarily for camouflage and signalling), as for bristles, down feathers and mammalian hairs[29–32]. Type 1, 2 and 4 filaments could shape a filamentous covering around the body and wings (Fig. 4) that might have functioned in streamlining the body surface to reduce drag during flight, as for modern bat fur or avian covert feathers[31,33]. Type 1 and 2 filaments occur in considerably high densities, particularly around the neck, shoulder, hindlimb and tail regions where the high degree of superposition prevents easy discrimination of adjacent fibres. This, along with the wide distribution and frayed appearance, resembles mammalian underfur adapted for thermal insulation[34,35]. Despite the less dense packing of type 4 filaments on the wings, the morphology of the structures is consistent with a thermoregulatory function: down feathers can achieve similar insulation to mammalian hair with only about half the mass, due to their air-trapping properties and high mechanical resilience, and are effective in retaining an insulating layer of still air[36]. This may optimize the encumbrance of the large wing area to wing locomotion[16]. Type 3 filaments around the jaw (Fig. 4) may have had tactile functions in, for example, prey handling, information gathering during flight, and navigation in nest cavities and on the ground at night, similar to bristles in birds[37].

Methods

Sampling. The specimen NJU–57003 is represented by two fragmented slabs, both containing original bone, fossilized soft tissues and natural moulds of bones. Each slab was glued together along the fissures by fossil dealers with the fossil on the surfaces untouched. The specimen CAGS–Z070 is represented by a single unbroken slab. Small flakes (1–3 mm wide) of samples with preserved integument and/or enclosing sediments were carefully removed from the inferred integumentary filaments from different parts of NJU–57003 (Supplementary Figs. 1a and 4a–c) using a dissecting scalpel. This method was used to avoid sampling from degraded products of other tissues, such as dermis, epidermis or even internal organs. Most samples were not treated further; the remainder were sputter-coated with gold to enhance SEM resolution (Fig. 2g,h and Supplementary Figs. 4a–f and 6). All of the experiments described below were repeated to validate the results.

SEM. Samples were examined using a JEOL 8530F Hyperprobe at the School of Earth Sciences, University of Bristol, and an LEO 1530VP scanning electron microscope at the Technical Services Centre, Nanjing Institute of Geology and Palaeontology, Chinese Academy of Sciences. Both instruments were equipped with a secondary electron detector, back-scattered electron detector and energy-dispersive X-ray spectrometer.

Measurements of melanosomes. The geometry of melanosomes was measured from SEM images using the image-processing programme ImageJ (available for download at http://rsbweb.nih.gov/ij/). We measured the maximum short and long axis lengths of melanosomes that were oriented perpendicular to line of sight. From these data, we calculated the mean and coefficient of variation of the long and short axis, and mean aspect ratio (long:short axis). Based on the proposed taphonomic alteration of fossil melanosome size (shrinkage up to ~20% in both length and diameter)[38,39], we modelled potential diagenetic alteration by enlarging the original measurements by 20%.

FTIR microspectroscopy. Samples of the filamentous tissues and associated sediments were removed separately from NJU–57003 and placed on a BaF_2 plate without further treatment. The infrared absorbance spectra were collected using a Nicolet iN10 MX infrared microscope (Thermo Fisher Scientific) with a cooled HgCdTe detector, at the School of Earth Sciences, University of Bristol. The microscope was operated in transmission mode with a 15 μm × 15μm aperture. Ten spectra were obtained from the filamentous tissues. The spectra show consistent results. The example presented in Fig. 2 shows the highest signal-to-noise ratio and was obtained with 2 cm^{-1} resolution and 2,000 scans.

Fluorescence microscopy. Selected areas with extensive soft tissue preservation in NJU–57003 were investigated and photographed using a Zeiss Axio Imager Z2 microscope with a digital camera (AxioCam HRc) and fluorescence illuminator (514 nm light-emitting diode) attached, at the Technical Services Centre, Nanjing Institute of Geology and Palaeontology, Chinese Academy of Sciences.

Laser-stimulated fluorescence imaging and data reduction protocol. Laser-stimulated fluorescence images were collected using the protocol of Kaye and co-workers[40,41]. NJU–57003 was imaged with a 405 nm 500 mW laser that was projected into a vertical line by a Laserline Optics Canada lens. The laser line was

swept repeatedly over the specimen during the exposure time for each image in a dark room. Images were captured with a Nikon D610 digital single-lens reflex camera fitted with an appropriate long-pass blocking filter in front of the lens to prevent image saturation by the laser. Standard laser safety protocols were followed during laser usage. The images were post-processed in Photoshop CS6 for sharpness, colour balance and saturation.

Phylogenetic macroevolutionary analysis. To analyse the evolution of feather characters, data were compiled on known integumentary characters across dinosaurs and pterosaurs. The basic data were taken from the supplementary data of Barrett et al.[2], comprising 84 dinosaurs (33 ornithischians, 7 sauropods and 44 theropods (including 4 Mesozoic birds)). To this dataset, we added four pterosaurs. Barrett et al.[2] scored taxa for three integumentary states (scales, filaments and feathers) in their macroevolutionary analyses. We checked and followed these basic categories and added three more. We then cross-referenced these six categories against the feather morphotypes defined by Xu et al.[42] The categories used herein are: scales (1; not included in Xu et al.[42]), monofilaments (2; morphotypes 1 and 2 in Xu et al.[42]), brush-like filaments associated with a planar basal feature (3; morphotypes 4 and 6 in Xu et al.[42]), tufts of filaments joined basally (4; morphotype 3 in Xu et al.[42]), open pennaceous vane, lacking secondary branching (5; morphotype 5 in Xu et al.[42]) and closed pennaceous feathers comprising a rachis-like structure associated with lateral branches (barbs and barbules) (6). There was some uncertainty over feathers coded herein as type 3, which could correspond to morphotype 6, or morphotypes 4 and 6 in Xu et al.[42]. However, the only taxa coded with these as the most derived feather type are *Sordes pilosus* and *Beipiaosaurus inexpectus*. These taxa belong to separate clades; thus, the calculation of ancestral states is not affected by how our feather type 3 is coded (that is, whether treating morphotypes 4 and 6 of Xu et al.[42] in combination or separately).

As in previous studies[2], we used maximum-likelihood approaches to explore trait evolution. There are many methods to estimate ancestral states for continuous characters, but choices are more limited for discrete characters, such as here, where only maximum-likelihood estimation of ancestral states is appropriate[43]. We calculated maximum-likelihood reconstructions of ancestral character states using the 'ace' function of the ape R package[44], with tree branch lengths estimated in terms of time, derived using the 'timePaleoPhy' function in the paleotree package[45] and the 'DatePhylo' function in the strap R package[46]. These enabled us to assess the results according to three methods of estimating branch lengths: the 'basic' method, which makes each internal node in a tree the age of its oldest descendant; 'equal branch length' (equal) method, which adds a pre-determined branch length (often 1 Myr) to the tree root and then evenly distributes zero-length branches at the base of the tree; and minimum branch length method, which minimizes inferred branching times and closely resembles the raw, time-calibrated tree. A problem with the 'basic' branch length estimation is that it results in many branch lengths of length zero, in cases where many related taxa are of the same age. In these cases, we added a line of code to make such zero branch lengths equal to 1/1,000,000 of the total tree length. A criticism of the minimum branch length method is that it tends to extend terminal branching events back in time, especially when internal ghost lineages are extensive[2], but this is not the case here, and the base of the tree barely extends to the Triassic–Jurassic boundary.

We ran our analyses using three evolutionary models with different rates of transition between the specified number of character states (six here)—namely, an equal-rates model, an all-rates-different model and a symmetrical model. These were calculated using the ace function in ape[2] and the add.simmap.legend function of the R package 'phytools'[47].

In a further series of analyses, we attempted a different approach to the ancestral state modelling, by recording all feather type traits found in each taxon (see Supplementary Results), so coding multiple trait values for taxa that preserve multiple feather types. This did not shed much light on patterns of evolution of feather types because the multiple trait codings (for example, 1,2 or 2,5,6) were each made into a new state, making 14 in all, and these were not linked. Therefore, the six multiply coded taxa that each had feather type 6 were represented as six independent states and their evolution was tracked in those terms. Furthermore, we attempted to separate the six characters so they would track through the tree whether recorded as singles or multiples in different taxa; however, we did not have the information to enable us to do this with confidence because of gaps in the coding. In terms of reality, these multiply coded taxa still represent an incomplete sample of the true presence and absence of character states. By chance, many coelurosaurs are not coded for scales (1) or monofilaments (2); yet, it is likely they all had these epidermal appendages. Therefore, attempting to run such multiple codings, with characters either as groups or coded independently, encounters so many gaps that the result is hard to interpret. Our approach is to code the most derived feather in each taxon. This is also incomplete because of fossilization gaps, but at least it represents a minimal, or conservative, approach to trait coding and hence to the discoveries of macroevolutionary patterns of feather evolution. Complete fossil data might show wider distributions of each feather type and hence deeper hypothesized points of origin. Complete coding of feather types would of course allow each trait to be tracked in a multiple-traits analysis.

Reporting Summary. Further information on research design is available in the Nature Research Reporting Summary linked to this article.

Data availability

The data that support the findings of this study are available in the Supplementary Information.

Received: 27 April 2018; Accepted: 23 October 2018;
Published online: 17 December 2018

References

1. Lucas, A. M. S. & Peter, R. *Avian Anatomy: Integument* (US Agricultural Research Service, Washington DC, 1972).
2. Barrett, P. M., Evans, D. C. & Campione, N. E. Evolution of dinosaur epidermal structures. *Biol. Lett.* **11**, 20150229 (2015).
3. Xu, X. et al. An integrative approach to understanding bird origins. *Science* **346**, 1253293 (2014).
4. Di-Poï, N. & Milinkovitch, M. C. The anatomical placode in reptile scale morphogenesis indicates shared ancestry among skin appendages in amniotes. *Sci. Adv.* **2**, e1600708 (2016).
5. Chen, C. F. et al. Development, regeneration, and evolution of feathers. *Annu. Rev. Anim. Biosci.* **3**, 169–195 (2015).
6. Mayr, G., Pittman, M., Saitta, E., Kaye, T. G. & Vinther, J. Structure and homology of *Psittacosaurus* tail bristles. *Palaeontology* **59**, 793–802 (2016).
7. Zheng, X. T., You, H. L., Xu, X. & Dong, Z. M. An Early Cretaceous heterodontosaurid dinosaur with filamentous integumentary structures. *Nature* **458**, 333–336 (2009).
8. Godefroit, P. et al. A Jurassic ornithischian dinosaur from Siberia with both feathers and scales. *Science* **345**, 451–455 (2014).
9. Kellner, A. W. et al. The soft tissue of *Jeholopterus* (Pterosauria, Anurognathidae, Batrachognathinae) and the structure of the pterosaur wing membrane. *Proc. R. Soc. B* **277**, 321–329 (2010).
10. Sharov, A. G. New flying reptiles from the Mesozoic of Kazakhstan and Kirgizia [in Russian]. *Tr. Inst. Palaeontol. Akad. Nauk SSSR* **130**, 104–113 (1971).
11. Czerkas, S. A. & Ji, Q. in *Feathered Dinosaurs and the Origin of Flight* (ed. Czerkas, S. J.) 15–41 (The Dinosaur Museum, Blanding, 2002).
12. Unwin, D. M. & Bakhurina, N. N. *Sordes pilosus* and the nature of the pterosaur flight apparatus. *Nature* **371**, 62–64 (1994).
13. Ji, Q. & Yuan, C. Discovery of two kinds of protofeathered pterosaurs in the Mesozoic Daohugou Biota in the Ningcheng region and its stratigraphic and biologic significances. *Geol. Rev.* **48**, 221–224 (2002).
14. Xu, X., Zhou, Z., Sullivan, C., Wang, Y. & Ren, D. An updated review of the Middle–Late Jurassic Yanliao Biota: chronology, taphonomy, paleontology and paleoecology. *Acta Geol. Sin.* **90**, 2229–2243 (2016).
15. Unwin, D. M. On the phylogeny and evolutionary history of pterosaurs. *Geol. Soc. Lond. Spec. Publ.* **217**, 139–190 (2003).
16. Frey, E., Tischlinger, H., Buchy, M. C. & Martill, D. M. New specimens of Pterosauria (Reptilia) with soft parts with implications for pterosaurian anatomy and locomotion. *Geol. Soc. Lond. Spec. Publ.* **217**, 233–266 (2003).
17. Lindgren, J. et al. Interpreting melanin-based coloration through deep time: a critical review. *Proc. R. Soc. B* **282**, 20150614 (2015).
18. Lindgren, J. et al. Molecular composition and ultrastructure of Jurassic paravian feathers. *Sci. Rep.* **5**, 13520 (2015).
19. Barden, H. E. et al. Morphological and geochemical evidence of eumelanin preservation in the feathers of the Early Cretaceous bird, *Gansus yumenensis*. *PLoS ONE* **6**, e25494 (2011).
20. Bendit, E. Infrared absorption spectrum of keratin. I. Spectra of α-, β-, and supercontracted keratin. *Biopolymers* **4**, 539–559 (1966).
21. Martinez-Hernandez, A. L., Velasco-Santos, C., De Icaza, M. & Castano, V. M. Microstructural characterisation of keratin fibres from chicken feathers. *Int. J. Envir. Pollut.* **23**, 162–178 (2005).
22. Liu, Y. et al. Comparison of structural and chemical properties of black and red human hair melanosomes. *Photochem. Photobiol.* **81**, 135–144 (2005).
23. Alibardi, L. Adaptation to the land: the skin of reptiles in comparison to that of amphibians and endotherm amniotes. *J. Exp. Zool.* **298B**, 12–41 (2009).
24. Kreplak, L., Doucet, J., Dumas, P. & Briki, F. New aspects of the α-helix to β-sheet transition in stretched hard α-keratin fibers. *Biophys. J.* **87**, 640–647 (2004).
25. Yassine, W. et al. Reversible transition between α-helix and β-sheet conformation of a transmembrane domain. *Biochim. Biophys. Acta – Biomembr.* **1788**, 1722–1730 (2009).
26. Xu, X. et al. A bizarre Jurassic maniraptoran theropod with preserved evidence of membranous wings. *Nature* **521**, 70–73 (2015).
27. Donoghue, P. C. J. & Benton, M. J. Rocks and clocks: calibrating the Tree of Life using fossils and molecules. *Trends Ecol. Evol.* **22**, 424–431 (2007).
28. Baron, M. G., Norman, D. B. & Barrett, P. M. A new hypothesis of dinosaur relationships and early dinosaur evolution. *Nature* **543**, 501–506 (2017).
29. Persons, W. S. IV & Currie, P. J. Bristles before down: a new perspective on the functional origin of feathers. *Evolution* **69**, 857–862 (2015).
30. Ruxton, G. D., Persons, W. S. IV & Currie, P. J. A continued role for signaling functions in the early evolution of feathers. *Evolution* **71**, 797–799 (2017).

31. Bullen, R. D. & McKenzie, N. L. The pelage of bats (Chiroptera) and the presence of aerodynamic riblets: the effect on aerodynamic cleanliness. *Zoology* **111**, 279–286 (2008).
32. Caro, T. The adaptive significance of coloration in mammals. *Bioscience* **55**, 125–136 (2005).
33. Homberger, D. G. & de Silva, K. N. Functional microanatomy of the feather-bearing integument: implications for the evolution of birds and avian flight. *Am. Zool.* **40**, 553–574 (2000).
34. Scholander, P., Walters, V., Hock, R. & Irving, L. Body insulation of some arctic and tropical mammals and birds. *Biol. Bull.* **99**, 225–236 (1950).
35. Ling, J. K. Pelage and molting in wild mammals with special reference to aquatic forms. *Q. Rev. Biol.* **45**, 16–54 (1970).
36. Gao, J., Yu, W. & Pan, N. Structures and properties of the goose down as a material for thermal insulation. *Text. Res. J.* **77**, 617–626 (2007).
37. Cunningham, S. J., Alley, M. R. & Castro, I. Facial bristle feather histology and morphology in New Zealand birds: implications for function. *J. Morphol.* **272**, 118–128 (2011).
38. McNamara, M. E., Briggs, D. E. G., Orr, P. J., Field, D. J. & Wang, Z. Experimental maturation of feathers: implications for reconstructions of fossil feather colour. *Biol. Lett.* **9**, 20130184 (2013).
39. Colleary, C. et al. Chemical, experimental, and morphological evidence for diagenetically altered melanin in exceptionally preserved fossils. *Proc. Natl Acad. Sci. USA* **112**, 12592–12597 (2015).
40. Wang, X. et al. Basal paravian functional anatomy illuminated by high-detail body outline. *Nat. Commun.* **8**, 14576 (2017).
41. Kaye, T. G. et al. Laser-stimulated fluorescence in paleontology. *PLoS ONE* **10**, e0125923 (2015).
42. Xu, X., Zheng, X. & You, H. Exceptional dinosaur fossils show ontogenetic development of early feathers. *Nature* **464**, 1338–1341 (2010).
43. Pagel, M. Detecting correlated evolution on phylogenies: a general method for the comparative analysis of discrete characters. *Proc. R. Soc. Lond. B* **255**, 37–45 (1994).
44. Paradis, E. *Analysis of Phylogenetics and Evolution with R* (Springer Science & Business Media, New York, 2011).
45. Bapst, D. W. paleotree: an R package for paleontological and phylogenetic analyses of evolution. *Methods Ecol. Evol.* **3**, 803–807 (2012).
46. Bell, M. A. & Lloyd, G. T. strap: an R package for plotting phylogenies against stratigraphy and assessing their stratigraphic congruence. *Palaeontol.* **58**, 379–389 (2015).
47. Revell, L. J. phytools: an R package for phylogenetic comparative biology (and other things). *Methods Ecol. Evol.* **3**, 217–223 (2012).

Acknowledgements

We thank Q. Ji, S. Ji and H. Huang for access to the specimen CAGS–Z070, as well as S. C. Kohn, Y. Fang, C. Wang and T. He for laboratory assistance. This work was supported by the National Natural Science Foundation of China (41672010 and 41688103) and Strategic Priority Research Program (B) of the Chinese Academy of Sciences (XDB26000000) to B.J., Research Grant Council of Hong Kong-General Research Fund (17103315) to M.P., ERC-StG-2014-637691-ANICOLEVO to M.E.M. and Natural Environment Research Council Standard Grant NE/1027630/1 to M.J.B.

Author contributions

B.J. and M.J.B. designed the research. Z.Y., B.J. and X.X. systematically studied the specimens. Z.Y., S.L.K., M.E.M. and P.J.O. performed the SEM analysis. Z.Y. and B.J. performed the FTIR analysis. M.P. and T.G.K. performed the laser-stimulated fluorescence imaging, data reduction and interpretation. M.J.B. performed the maximum-likelihood analyses. Z.Y., B.J., M.J.B., M.E.M., X.X. and P.J.O. wrote the paper. All authors approved the final draft of the paper.

Competing interests

The authors declare no competing interests.

Additional information

Supplementary information is available for this paper at https://doi.org/10.1038/s41559-018-0728-7.

Reprints and permissions information is available at www.nature.com/reprints.

Correspondence and requests for materials should be addressed to B.J. or M.J.B.

Publisher's note: Springer Nature remains neutral with regard to jurisdictional claims in published maps and institutional affiliations.

nature research

Corresponding author(s): Baoyu Jiang and Michael J. Benton

Reporting Summary

Nature Research wishes to improve the reproducibility of the work that we publish. This form provides structure for consistency and transparency in reporting. For further information on Nature Research policies, see Authors & Referees and the Editorial Policy Checklist.

Statistical parameters

When statistical analyses are reported, confirm that the following items are present in the relevant location (e.g. figure legend, table legend, main text, or Methods section).

n/a	Confirmed	
☐	☒	The exact sample size (*n*) for each experimental group/condition, given as a discrete number and unit of measurement
☐	☒	An indication of whether measurements were taken from distinct samples or whether the same sample was measured repeatedly
☒	☐	The statistical test(s) used AND whether they are one- or two-sided *Only common tests should be described solely by name; describe more complex techniques in the Methods section.*
☒	☐	A description of all covariates tested
☐	☒	A description of any assumptions or corrections, such as tests of normality and adjustment for multiple comparisons
☐	☒	A full description of the statistics including central tendency (e.g. means) or other basic estimates (e.g. regression coefficient) AND variation (e.g. standard deviation) or associated estimates of uncertainty (e.g. confidence intervals)
☒	☐	For null hypothesis testing, the test statistic (e.g. *F*, *t*, *r*) with confidence intervals, effect sizes, degrees of freedom and *P* value noted *Give P values as exact values whenever suitable.*
☒	☐	For Bayesian analysis, information on the choice of priors and Markov chain Monte Carlo settings
☒	☐	For hierarchical and complex designs, identification of the appropriate level for tests and full reporting of outcomes
☒	☐	Estimates of effect sizes (e.g. Cohen's *d*, Pearson's *r*), indicating how they were calculated
☒	☐	Clearly defined error bars *State explicitly what error bars represent (e.g. SD, SE, CI)*

Our web collection on statistics for biologists may be useful.

Software and code

Policy information about availability of computer code

Data collection	ImageJ (available for download at http:// rsbweb.nih.gov/ij/); Photoshop CS6
Data analysis	R (available for download at https://cran.r-project.org) and R packages: ape, paleotree, strap and phytools.

For manuscripts utilizing custom algorithms or software that are central to the research but not yet described in published literature, software must be made available to editors/reviewers upon request. We strongly encourage code deposition in a community repository (e.g. GitHub). See the Nature Research guidelines for submitting code & software for further information.

Data

Policy information about availability of data

All manuscripts must include a data availability statement. This statement should provide the following information, where applicable:

- Accession codes, unique identifiers, or web links for publicly available datasets
- A list of figures that have associated raw data
- A description of any restrictions on data availability

The data that support the findings of this study are available from the corresponding authors upon reasonable request.

Field-specific reporting

Please select the best fit for your research. If you are not sure, read the appropriate sections before making your selection.

☐ Life sciences ☐ Behavioural & social sciences ☒ Ecological, evolutionary & environmental sciences

For a reference copy of the document with all sections, see nature.com/authors/policies/ReportingSummary-flat.pdf

Ecological, evolutionary & environmental sciences study design

All studies must disclose on these points even when the disclosure is negative.

Study description	We examined the integumentary structures of two pterosaur specimens, including morphology of the structures, geometry of constituent melanosomes and FTIR analysis, and explored the evolution of feather characters using maximum-likelihood approach.
Research sample	The studied fossil specimens possess the best-preserved integumentary structures yet described in pterosaurs, coming from the Middle Jurassic Yanliao Biota of China. Both specimens represents anurognathid pterosaurs, and possibly juveniles.
Sampling strategy	Samples prepared for SEM and FTIR analyses were small flakes (1–3 mm wide) with preserved integument and/or enclosing sediments. All body parts that preserved integument were sampled, including head, forelimb, hindlimb, and tail.
Data collection	The geometry of melanosomes was measured from SEM images using the image-processing program ImageJ (available for download at http:// rsbweb.nih.gov/ij/). We measured maximum short and long axis length of melanosomes that were oriented perpendicular to line of sight. In macroevolutionary analysis, The basic data were taken from the Supplementary data of Barrett et al. 2015, comprising 74 dinosaurs (33 ornithischians, seven sauropods and 44 theropods (including four Mesozoic birds)); to this dataset we added four pterosaurs.
Timing and spatial scale	Measurements of melanosomes were conducted during January 2016–May 2017, and Data for macroevolutionary analysis were compiled during December 2016–March 2017.
Data exclusions	No data were excluded from the analyses.
Reproducibility	All experiments were repeated in order to validate the results.
Randomization	Samples for SEM and FTIR analyses were not randomly taken from the specimen due to originally patchy distribution of the integumentary structures.
Blinding	Not relevant to our study because no live participants were involved.

Did the study involve field work? ☐ Yes ☒ No

Reporting for specific materials, systems and methods

Materials & experimental systems

n/a	Involved in the study
☒	☐ Unique biological materials
☒	☐ Antibodies
☒	☐ Eukaryotic cell lines
☐	☒ Palaeontology
☒	☐ Animals and other organisms
☒	☐ Human research participants

Methods

n/a	Involved in the study
☒	☐ ChIP-seq
☒	☐ Flow cytometry
☒	☐ MRI-based neuroimaging

Palaeontology

Specimen provenance	Both specimens belong to the Middle Jurassic Yanliao Biota of China. NJU–57003 comes from the Mutoudeng locality, Hebei Province, and CAGS–Z070 comes from the Daohugou locality, Inner Mongolia.
Specimen deposition	Both specimens are in public, accessible, recognised repositories. NJU–57003 is hosted in Nanjing University, and CAGS–Z070 is hosted in Institute of Geology, Chinese Academy of Geological Sciences.

Dating methods | No new dates are provided.

☐ Tick this box to confirm that the raw and calibrated dates are available in the paper or in Supplementary Information.